

SPACE VECTOR PULSE WIDTH MODULATION OF THREE-LEVEL INVERTER EXTENDING OPERATION INTO OVERMODULATION REGION

Subrata K. Mondal, *Member, IEEE*, Bimal K. Bose, *Life Fellow, IEEE*, Valentin Oleschuk,
and Joao O. P. Pinto, *Student Member, IEEE*
Department of Electrical and Computer Engineering
The University of Tennessee
Knoxville, TN 37996-2100

Abstract - Multi-level voltage-fed inverters with space vector pulse width modulation have established their importance in high power high performance industrial drive applications. The paper proposes an overmodulation strategy of space vector PWM of a three-level inverter with linear transfer characteristic that easily extends from the undermodulation strategy previously developed by the authors for neural network implementation. The overmodulation strategy is very complex because of large number of inverter switching states, and hybrid in nature, that incorporates both undermodulation and overmodulation algorithms. The paper describes the algorithm development, system analysis, DSP based implementation, and evaluation study to validate the modulator performance. The modulator takes the command voltage and angle information at the input and generates symmetrical PWM waves for the three phases of an IGBT inverter that operates at 1.0 kHz switching frequency. The switching states are distributed such that the neutral point voltage always remains balanced. An open loop volts/Hz controlled induction motor drive has been evaluated extensively by smoothly varying the voltage and frequency in the whole speed range that covers both undermodulation and overmodulation regions, and performance was found to be excellent. The PWM algorithm can be easily extended to vector-controlled drive.

1. INTRODUCTION

Three-level voltage-fed PWM inverters are recently showing growing popularity for multi-megawatt industrial drive applications. The main reasons for this popularity are easy sharing of large voltage between the series devices and improvement of harmonic quality at the output compared to a two-level inverter. In the lower end of power, GTO devices are being replaced by IGBTs because of their rapid evolution in voltage and current ratings and higher switching frequency. The space vector PWM (SVM) of a three-level inverter provides the additional advantages of superior harmonic quality and larger undermodulation range that extends the modulation factor to 90.7% from the traditional value of 78.5% in sinusoidal PWM. However, space vector PWM of a three-level inverter is considerably more complex than that of a two-level inverter because of large number of inverter switching states[1]. In addition, there is the problem of neutral point voltage balancing.

In the past, a number of papers were published [2]-[5] describing SVM algorithms in the undermodulation range and their digital signal processor (DSP) based implementation. Recently, the authors described [6] a neural network based SVM of a three-level inverter in the undermodulation range for an induction motor drive. Unfortunately, operation in the undermodulation range of SVM restricts the drive operation in constant torque region only with voltage modulation factor up to 90.7%. An overmodulation strategy of SVM with modulation factor extending from 90.7% to near unity is essential if the drive is required to operate at extended speed including the field-weakening region in vector control with higher torque and power characteristics. The overmodulation strategy of a two-level inverter and its neural network implementation were described in the literature [7][8].

This paper describes an overmodulation strategy of space vector PWM of a three-level inverter that extends from the undermodulation strategy previously described by the authors for neural network implementation. Following the description of overmodulation strategy, the system analysis, algorithm development and DSP based implementation have been discussed. Finally, the modulator operation has been validated by extensive evaluation on an open loop volts/Hz controlled induction motor drive.

2. SVM OPERATION IN UNDERMODULATION REGION

The overmodulation strategy of a three-level inverter to be described in the paper is somewhat hybrid in nature, i.e., it incorporates the undermodulation strategy in part of a cycle. Therefore, for completeness, the undermodulation strategy described in the previous paper [6] will be briefly reviewed and will then be extended into the overmodulation region. Fig. 1 shows the schematic diagram of a three-level voltage-fed IGBT inverter with induction motor load and space vector PWM based open loop volts/Hz control in the lower part of the figure. For three-phase ac-dc-ac power conversion, a similar inverter unit is connected at the input in inverse manner. The phase U , for example, is in state P (positive bus voltage) when the switches S_{1U} and S_{2U} are

closed, whereas it is in N state (negative bus voltage) when S_{3U} and S_{4U} are closed. At neutral point clamping, the phase is in O state when either S_{2U} or S_{3U} conducts depending on positive or negative phase current polarity, respectively. For neutral point voltage balancing, the average current injected at O should be zero. The SVM controller is indicated in the control block diagram. It receives the voltage ($V_{qs}^* = V^*$) and angle (θ_e^*) command signals at the input as shown and generates the PWM pulses for the inverter. For a vector-controlled drive with synchronous current control [1], both V_{qs}^* and V_{ds}^* signals are present and the unit vector signal (θ_e^*) can be generated in feedback (for direct vector control) or feedforward (for indirect vector control) manner. As the frequency or speed command signal ω_e^* is gradually increased from zero, the SVM first operates in undermodulation region, and then smoothly transitions into overmodulation region with linear voltage transfer characteristic in the overmodulation range until square-wave operation is attained. Of course, a three-level inverter can not operate in square-wave mode (modulation factor $m = 1$) because it will then lose the three level switching characteristics. It should be mentioned here that for the line-side converter (or rectifier) in ac-dc-ac conversion, the SVM algorithm should be restricted to undermodulation region only.

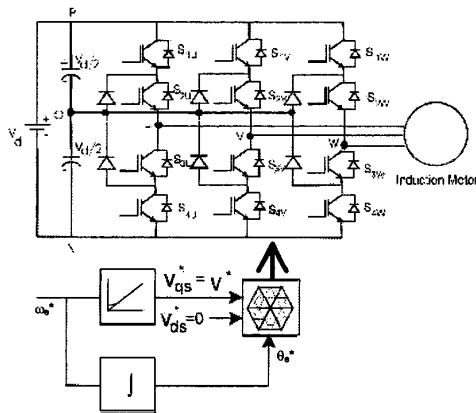


Fig.1. Three-Level inverter induction motor drive with space vector PWM based volts/Hz Control

A three-level inverter is characterized by $3^3 = 27$ switching states as indicated in Fig. 2(a) where each phase can have P , N or O state. There are 24 active states, and the remaining three are zero states (PPP , OOO , NNN) that lie at the center of the hexagon. The area of the hexagon can be divided into six sectors (A to F) and each sector has four regions (1 to 4) giving altogether 24 regions of operation. The command voltage (V^*) trajectory, given by circle, can expand from zero to that inscribed in the large hexagon in the upper limit of the undermodulation range. At this limit, the modulation factor $m = 0.907$, where $m = V^*/V_{1sw}$ (V^* = command or reference voltage magnitude and V_{1sw} = peak value of phase fundamental voltage at square wave

condition). Fig. 2(a) shows a smaller circle embracing the region 1 of all the sectors which is defined as undermodulation mode-1. The large circle beyond region 1 that embraces regions 2, 3 and 4 of all the sectors is defined as undermodulation mode-2. In undermodulation region, the nearest three inverter voltage vectors that coincide with the apexes of the triangle are selected and the corresponding time segments are calculated to construct the PWM wave. For example, if V^* is located in region 3 of sector A as shown, the switching vectors V_1 , V_3 and V_4 are selected and the corresponding time segments T_a , T_b and T_c (see Fig. 2(b)) are calculated. These time segments are then distributed in a certain sequence in the sampling period (T_s) so that the PWM wave is symmetrical and the neutral point voltage remains balanced. The transfer characteristic between the fundamental output voltage and the command voltage is inherently linear in the whole undermodulation range.

3. SVM OPERATION IN OVERMODULATION REGION

The inherently nonlinear operation in overmodulation region starts when the reference voltage V^* exceeds the hexagon boundary. The SVM overmodulation strategy of three-level inverter has some similarity with that of a two-level inverter which was described in [8]. The principle of overmodulation is similar in all the sectors, and therefore, we will highlight the operation for sector A only. In overmodulation mode-1, shown in Fig. 2(b) for the sector A, V^* crosses the hexagon side at two points. To compensate the loss of fundamental voltage, i.e., to track the output fundamental voltage with the reference voltage, a modified reference voltage trajectory is selected that remains partly on the hexagon and partly on a circle. The circular part of the trajectory, shown by the segments ab and de has larger radius V_m^* ($V_m^* > V^*$) and crosses the hexagon at angle θ , as shown in the figure. The expression of V_m^* , as function of crossover angle θ [8], can be given as

$$V_m^* = \frac{2V_d(\frac{\pi}{6} - \theta)}{\pi \sin(\frac{\pi}{6} - \theta)} \dots\dots\dots (1)$$

where V_d = dc link voltage. In the circular segment, the undermodulation strategy, as discussed before, remains valid. For example, in the ab segment, the inverter vectors V_1 , V_2 and V_3 vectors are selected for the corresponding time segments T_a , T_c and T_b , respectively. Similarly, for the de segment, the vectors V_4 , V_3 and V_5 are selected and the respective time segments are T_c , T_b and T_a . The trajectory segment bd on the hexagon can be subdivided into two parts: bc and cd . In the bc segment, only the vectors V_2 and V_3 (see Fig. 2(a)) are selected for the corresponding time segments T_c and T_b , whereas in the segment cd , V_3 and V_5 vectors are selected for time segments T_b and T_a respectively. The

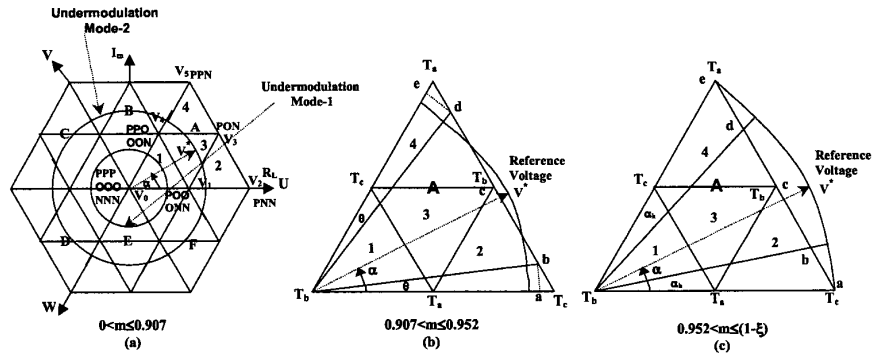


Fig.2.Space voltage vectors showing operations in undermodulation and overmodulation Regions

(a) Undermodulation operation (b) Overmodulation mode-1 operation (c) Overmodulation mode-2 operation

crossover angle θ decreases with higher modulation factor m until at the limit of mode-1 ($m = 0.952$), the trajectory lies entirely on the hexagon. For linear voltage transfer characteristic, the relation between θ and m is shown in Fig. 3(a) [8].

The overmodulation mode-2 starts when V^* or m increases further. The operation in this region, as shown in Fig. 2(c), is characterized by partly holding the hexagon corner vector for holding angle α_h and partly tracking the hexagon side (segments bc and cd) in every sector. During holding angle, the machine phase voltages remains constant, whereas during hexagon tracking the voltages change similar to that of mode-1 described above. The angle α_h increases with modulation factor until at the end of mode-2 ideal six-step or square-wave operation is attained when the modified vector is held at hexagon corners for 60° , i.e., $\alpha_h = 30^\circ$. For linear transfer characteristic, the relation between α_h and m is shown in Fig. 3(b) [8].

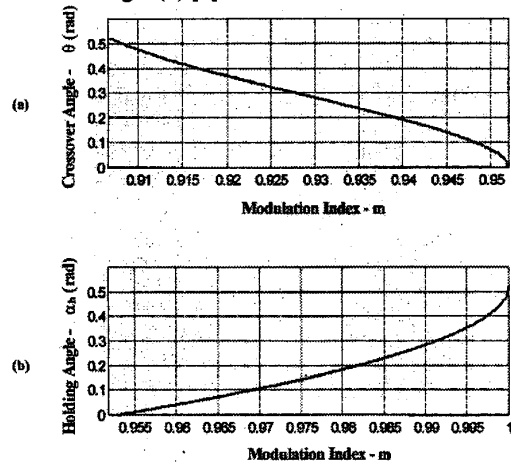


Fig.3.(a) Modulation factor (m) relation with crossover angle(θ) in overmodulation mode-1
(b) Modulation factor (m) relation with crossover angle(α_h) in overmodulation mode-2

A. Derivation of Time Segments of Inverter Voltage Vectors

As explained above, during modes 1 and 2 of overmodulation region, a significant part of operation occurs on the hexagon side in the sections bc in region 2 and cd in region 4. The analytical expressions for time segments in these sections will now be derived. Consider that the reference voltage V^* is tracking the section bc in region 2 as indicated in Fig. 4. Here the sector angle α is now replaced by the general trajectory angle θ_e . The following two equations should be valid for space vector PWM:

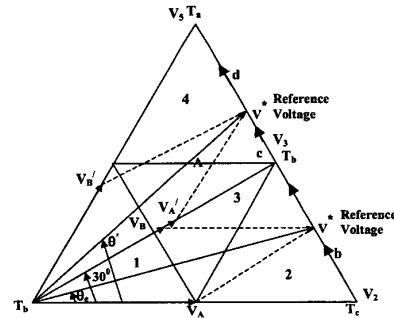


Fig.4.Derivation of time segments in Regions 2 and 4 of sector A for the trajectory on the hexagon

$$V_2.T_c + V_3.T_b = V^*.T_s / 2 \quad \dots\dots (2)$$

$$T_b + T_c = T_s / 2 \quad \dots\dots (3)$$

where T_s = sampling time. The voltage V^* can be resolved into component vectors V_A and V_B as shown in the figure. From the geometry we can write

$$\frac{V_B}{\sin\theta_e} = \frac{V^*}{\sin 150^\circ} = 2V^* \quad \dots\dots (4)$$

$$\frac{V_2}{\sin(120^\circ - \theta_e)} = \frac{V^*}{\sin 60^\circ} = \frac{2}{\sqrt{3}} V^* \dots\dots (5)$$

$$V_A = V^* \cos \theta_e - V_B \cos 30^\circ \dots\dots\dots (6)$$

Substituting (4) and (5) in (6) and simplifying, we get

$$V_A = V_2 \frac{\sqrt{3} \cos \theta_e - 3 \sin \theta_e}{\sqrt{3} \cos \theta_e + \sin \theta_e} \dots\dots\dots (7)$$

Since $\frac{T_c}{0.5T_s} = \frac{V_A}{V_2}$, we can write

$$T_c = \frac{T_s}{2} \left(\frac{\sqrt{3} \cos \theta_e - 3 \sin \theta_e}{\sqrt{3} \cos \theta_e + \sin \theta_e} \right) \dots\dots\dots (8)$$

Therefore, to establish V_b , the vector V_3 has to be impressed for the time segment

$$T_b = \frac{T_s}{2} - T_c \dots\dots\dots (9)$$

as given by (3). Similar derivations can be made for region 2 in all the six sectors.

Now, consider the tracking segment cd in Fig. 4 where the following equations are valid:

$$V_3.T_b + V_5.T_a = V^* \cdot \frac{T_s}{2} \dots\dots (10)$$

$$T_b + T_a = \frac{T_s}{2} \dots\dots\dots (11)$$

Again, from the geometry, we can write

$$\frac{V_B'}{\sin(\theta_e' - 30^\circ)} = \frac{V^*}{\sin 150^\circ} = 2V^* \dots (12)$$

$$\frac{V_3}{\sin(120^\circ - \theta_e')} = \frac{V^*}{\sin 90^\circ} = V^* \dots\dots (13)$$

$$V_A' = V^* \cos(\theta_e' - 30^\circ) - V_B' \cos 30^\circ \dots\dots (14)$$

Substituting (12) and (13) in (14) and simplifying we can write

$$\frac{V_A'}{V_3} = \left(\frac{2\sqrt{3} \cos \theta_e' - 2 \sin \theta_e'}{\sqrt{3} \cos \theta_e' + \sin \theta_e'} \right) \dots\dots\dots (15)$$

where θ_e' is the new value of θ_e .

Since $\frac{T_b}{0.5T_s} = \frac{V_A'}{V_3}$, the time segments for V_3 and V_5 can be written respectively as

$$T_b = \frac{T_s}{2} \left(\frac{2\sqrt{3} \cos \theta_e' - 2 \sin \theta_e'}{\sqrt{3} \cos \theta_e' + \sin \theta_e'} \right) \dots\dots (16)$$

$$T_a = \frac{T_s}{2} - T_b \dots\dots\dots (17)$$

Similar calculations can also be made for region 4 in all the sectors.

B. Derivation of Turn-on Times

Once the analytical time segment expressions have been derived for hexagon tracking, it is possible to plot the PWM waveforms accurately in all the sectors as function of θ_e angle. Fig. 5(a) shows the typical PWM waves in sector A for the three phases in region 2 where the switching states (P; N, O) for segments T_c and T_b can be verified from Fig. 2(a). Note that the sequence of T_c and T_b is reversed in the next $T_s/2$ interval for symmetry of PWM waveform. The P and N state turn-on times of phase voltages are marked on the figure. The remaining interval corresponds to O state. For example, P state turn-on time of U phase (T_{UP-ON}) and N state turn-on time of W phase (T_{WN-ON}) are saturated at zero, whereas the N state turn-on time of V phase (T_{VN-ON}) (which has notched shape and is referred to center axis) has a finite value. Fig. 5(b) shows the corresponding PWM waves in region 4.

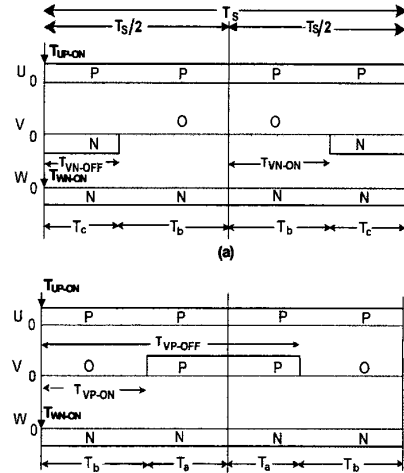


Fig.5. PWM waveforms showing sequence of switching states during hexagon tracking in overmodulation of sector A (a) Region 2, (b) Region 4

By drawing the waveform sketches for all the sectors in regions 2 and 4, we can derive the general expressions of P and N state turn-on time for all the phases, i.e., $T_{UP-ON(2)}$, $T_{UN-ON(2)}$, $T_{VP-ON(2)}$, $T_{VN-ON(2)}$, $T_{WP-ON(2)}$, $T_{WN-ON(2)}$, $T_{UP-ON(4)}$, $T_{UN-ON(4)}$, $T_{VP-ON(4)}$, $T_{VN-ON(4)}$, $T_{WP-ON(4)}$, $T_{WN-ON(4)}$ with the help of Fig.5. Because of waveform symmetry, the turn-off times of any phase can be given as

$$T_{P-OFF} = T_s - T_{P-ON} \dots\dots\dots (18)$$

$$T_{N-OFF} = \frac{T_s}{2} - T_{N-ON} \dots\dots (19)$$

The equations for T_{UP-ON} and T_{UN-ON} for regions 2 and 4, respectively, along with the equations of undermodulation

circular segments (ab and de)[6] for all the sectors in mode-1 are plotted, respectively, in Figs. 6(a) and 6(b). The corresponding curves for undermodulation (mode-1 and mode-2) [6] are also given in the figures for comparison. Note that the T_{UP-ON} curve in overmodulation mode-1 remains saturated at 0 in parts of sectors A and F, and at $T_s/2$ in sectors C and D and parts of B and E sectors. Similarly, the T_{UN-ON} curve remains saturated at 0 in parts of sectors C and D, and at $T_s/2$ in sectors A and F and parts of B and E sectors. The turn-on time profiles for other phases are identical but are mutually phase-shifted by $2\pi/3$ angles. As the modulation factor m increases, the crossover angle θ decreases and the greater amount of trajectory remains on the hexagon. This increases the saturation regions in sectors A, F and C, D and steepens the slope of nearly straight line segments in B and E sectors. Finally, as mentioned before, $\theta = 0$ and $m = 0.952$ at the end of mode-1.

In overmodulation mode-2, hexagon tracking occurs like mode-1, but crossover angle θ is replaced by the holding angle α_h during which the hexagon corner vector is held constant. In Fig.6, T_{UP-ON} and T_{UN-ON} will be fully saturated in sectors A, F, C and D, as indicated in the figure. Ultimately, with the increase of modulation factor, the curves become vertical in sectors B and E giving square-wave output. Of course, m is restricted to slightly lower than 1 (i.e., $1 - \xi$) to prevent square-wave operation.

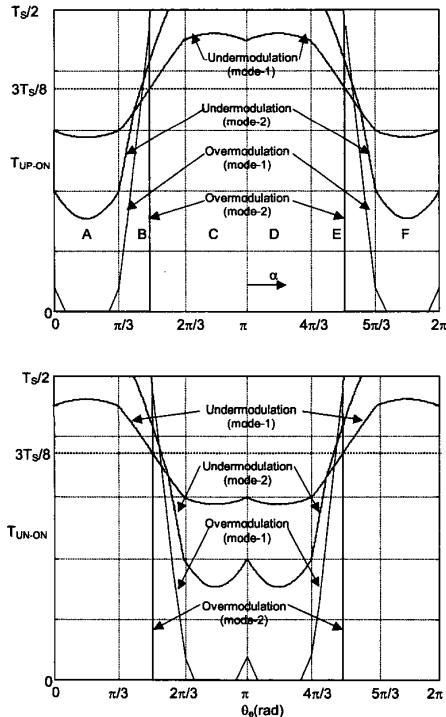


Fig.6. Calculated plots of turn-on time for phase U
(a) turn-on time for P state (T_{UP-ON})
(b) turn-on time for N state (T_{UN-ON})

4. DSP BASED SVM IMPLEMENTATION

Once the turn-on time expressions have been derived for all the phases in both P and N states, it is possible to evaluate them in real time, derive the corresponding digital words with the help of DSP and establish the PWM waves with the help of a timer. Again, in a practical converter application, the undermodulation algorithm has to be executed before extending to overmodulation region.

For digital implementation, the command voltage V^* and angle θ_e^* are sampled. Based on this information, the current sector is identified, the modulation factor m and α angle in the sector are calculated. The value of m identifies the particular mode of operation. If operation occurs in undermodulation mode (mode-1 and mode-2), the digital words WT_{P-ON} and WT_{N-ON} for all the phases are solved with the help of V^* and α^* information, and converted to corresponding pulse widths with the help of timer. If operation occurs in overmodulation mode-1, θ angle is solved from Fig. 3(a). If $\alpha < \theta$ or $\alpha > (\pi/3 - \theta)$ in a sector, the undermodulation mode is activated, but V^* is replaced by V_m^* (as shown in eqn. (1)). If α angle range is $\theta < \alpha < (\pi/3 - \theta)$, then WT_{P-ON} and WT_{N-ON} are generated for regions 2 and 4, and the corresponding pulse widths are generated with the timer. The overmodulation mode-2 is identified for $m > 0.952$ as indicated in the figure. The holding angle α_h is determined from Fig. 3(b) and the modified angle α_m is calculated with the help of current α angle. During holding, which is valid for $0 < \alpha^* < \alpha_h$ in region 2 and for $(\pi/3 - \alpha_h) < \alpha < \pi/3$ in region 4, WT_{P-ON} and WT_{N-ON} correspond to the corner vectors shown in Fig. 2, whereas during hexagon tracking these words are generated for regions 2 and 4, as discussed above. The sampling time T_s for digital implementation is 1.0 ms. that corresponds to the inverter switching frequency of 1.0 kHz.

5. PERFORMANCE EVALUATION

Once the complete algorithm for the PWM modulator was developed and debugged, it was evaluated extensively with an open loop volt/Hz controlled induction motor drive (100 hp, 2200 V, 60 Hz machine with $V_d = 3000$ V) (see Fig. 1) by smoothly varying the voltage and frequency in the whole speed range that covered both undermodulation and overmodulation regions (nearest to square-wave), and performance was found to be excellent. Figs. 7(b) and 7(c) show the line voltage (V_{UV}) and phase current (I_U) waves in overmodulation mode-1 and mode-2, respectively, indicating the dominance of lower order harmonics. Fig. 7(a) shows the undermodulation waves for comparison figure. The developed PWM algorithm can be easily extended for vector-controlled drive.

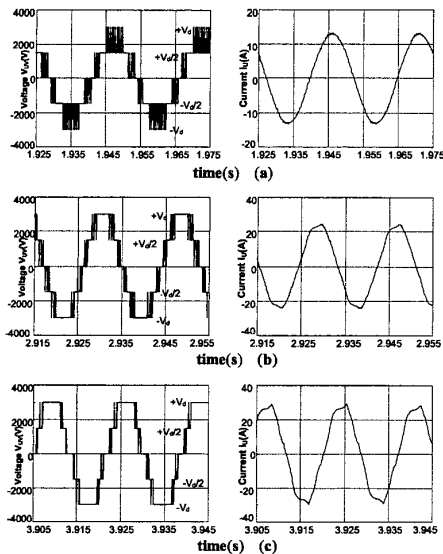


Fig. 7. Machine line voltage and phase current waves:
(a) Undermodulation (40 Hz)
(b) Overmodulation mode-1 (56 Hz)
(c) Overmodulation mode-2 (59 Hz)

6. CONCLUSION

The space vector PWM algorithm for a three-level voltage-fed inverter has been extended to overmodulation range in this project. The system analysis, algorithm development and its equivalent DSP based implementation have been described systematically in the paper. The overmodulation strategy easily blends with the undermodulation algorithm so that the inverter can operate smoothly from low speed to the extended speed range. Once the DSP based implementation strategy was developed, the modulator was evaluated extensively with open loop volts/Hz. controlled induction motor drive (100 hp, 2200 V, 60 Hz,) with dc link voltage $V_d = 3000$ V, and the performance was found to be excellent in both static and dynamic conditions. Currently, the modulator incorporating both the undermodulation and overmodulation strategies is being implemented in a neural network and the operation is

being extended to an indirect vector-controlled drive incorporating the field-weakening mode of operation.

ACKNOWLEDGMENT

The research described in this publication was made possible in part by Award No. ME2-3015 of the Moldovan Research and Development Association (MRDA) and the U.S. Civilian Research & Development Foundation for the Independent States of the Former Soviet Union (CRDF).

REFERENCES

- [1] B.K.Bose, *Modern Power Electronics and AC Drives*, Prentice Hall, Upper Saddle River, 2002.
- [2] H.L.Liu, N.S.Choi and G.H.Cho, "DSP based space vector PWM for three-level inverter with dc-link voltage balancing", IEEE IECON Conf. Rec., pp. 197-203, 1991.
- [3] M.Koyama, T.Fujii, R. Uchida and T.Kawabata, "Space voltage vector based new PWM method for large capacity three-level GTO inverter", IEEE IECON Conf. Rec., pp. 271-276, 1992.
- [4] J. Zhang, "High performance control of a three-level IGBT inverter fed ac drive", IEEE IAS Annu. Meet. Conf. Rec., pp. 22-28, 1995.
- [5] Y.H.Lee, B.S. Suh and D.S. Hyun, "A novel PWM scheme for a three-level voltage source inverter with GTO thyristors", IEEE Trans. Ind. Appl., vol. 32, pp. 260-268, March/April 1996.
- [6] S. K. Mondal, J.O.P. Pinto and B.K.Bose, "A neural network based space vector PWM controller for a three-level voltage-fed inverter induction motor drive", IEEE IAS Annu. Meet. Conf. Rec., pp. 1679-1686, 2001.
- [7] J. Holtz, W. Lotzkat and M. Khambadkone, "On continuous control of PWM inverters in the overmodulation range including the six-step mode", IEEE Trans. Power Electronics, vol. 8, pp. 546-553, Oct. 1993.
- [8] J.O.P.Pinto, B.K.Bose, L.E.B. da Silva and M.P.Kazmierkowski, "A neural network based space vector PWM controller for voltage-fed inverter induction motor drive", IEEE Trans. Ind. Appl., vol. 36, pp. 1628-36, Nov./Dec. 2000.